

# Observational constraints and diagnostics with error bars for time-dependent dark energy models

Hongchao Zhang, Enkun Li, and Lixin Xu\*

*Institute of Theoretical Physics, School of Physics and Optoelectronic Technology,  
Dalian University of Technology, Dalian, 116024, People's Republic of China*

In this work, three modified diagnostics with error bars via the error propagation equation are proposed and three time-dependent dark energy models are constrained by the cosmic observational data sets from *Planck* 2015, SNIa, BAO, OHD. Then we distinguish and judge three time-dependent dark energy models by using two combinations of diagnostic,  $S_3^{(1)}, S_4^{(1)}, \epsilon$  and  $S_5^{(1)}, S_5^{(2)}, \epsilon$ , with and without error bars respectively in terms of the new values of cosmological parameters. The diagnostics endowed with error bars contain more abundant information than those without error bars and should become a powerful instrument for models distinguishing and analysing. From the phase diagrams with error bars we can not only distinguish different models, but also compare their stability and robustness under the errors generating from the original parameters.

PACS numbers: 98.80.-k, 98.80.Es

## I. INTRODUCTION

Type Ia supernova (SNIa) observations [1, 2], cosmic microwave background (CMB) anisotropy measurement from Wilkinson Microwave Anisotropy Probe (WMAP) [3], and large scale structure from the Sloan Digital Sky Survey (SDSS) [4] show that our Universe is undergoing an accelerating expansion phase. These observations reveals that about 70% of cosmic components should be responsible for the last-time acceleration. In order to explain the mechanism behind this phenomenon, theorists introduced an exotic energy component with negative pressure, called dark energy. For recent reviews about dark energy, please see [5–11].

Based on this opinion, various of dark energy models have been proposed. Among all these models,  $\Lambda$ CDM model is the simplest and most attractive one at first [5]. In standard  $\Lambda$ CDM cosmology, the late-time cosmic acceleration is provided by a cosmological constant satisfying an equation of state (EOS)  $w \equiv P_{de}/\rho_{de} = -1$ . The latest released *Planck* 2015 data [12] shows that Planck spectra at high multipoles ( $l \gtrsim 40$ ) are extremely well described by the standard spatially-flat six-parameter  $\Lambda$ CDM cosmology with a power-law spectrum of adiabatic scalar perturbations. The results favour the base  $\Lambda$ CDM cosmology seemingly. Moreover, by combining *Planck* TT+lowP+lensing data with other astrophysical data, including JLA supernovae, the EOS of dark energy is constrained to  $w = -1.006 \pm 0.045$  [12]. This suggests that the observed Universe could be well described by  $\Lambda$ CDM model.

However, there are two thorny issues in  $\Lambda$ CDM cosmology, i.e. the ‘‘cosmic coincidence problem’’ and the ‘‘fine tuning problem’’. And the energy density of cosmological constant is 120 orders of magnitude smaller than expected from quantum field theory [13]. Consequently people proposed a lot of alternative dark energy models, for related articles, please see [14–29]. So many alternatives but no one has absolute advantage over the others. It becomes substantially important and constructive to discriminate them from the standard model or

one from the other via certain mechanism in order to find better scenarios.

It is known that the Hubble parameter,  $H \equiv \dot{a}/a$ , and the deceleration parameter,  $q \equiv -\ddot{a}/\dot{a}^2 = -\ddot{a}/aH^2$  are two elementary geometrical variables in cosmology, where  $a$  is the scalar factor and  $\cdot$  denotes the derivative to cosmic time  $t$ . Generally speaking, different models have different geometric behaviors, which can be represented by  $a(t)$  and these two geometrical variables. Sahni et al. [30, 31] proposed a geometrical diagnostic pair for dark energy, i.e. statefinder, which is constructed from  $a(t)$  and its derivatives up to the third order, can be regarded as natural promotion of  $H$  and  $q$ . The statefinder pair  $\{r, s\}$  define as follows

$$r = \frac{\ddot{a}}{aH^2}, \quad s = \frac{r-1}{3(q-1/2)}. \quad (1)$$

Since the statefinder was put forward, researchers have used it to discriminate a great deal of dark energy models [32–47]. Recently, Arabsalmani et al. [48] generalized the original statefinder to statefinder hierarchy  $S_n, S_n^{(1)}, S_n^{(2)}$ , which are constructed by higher derivatives of scale factor, then Wang and Meng [49] utilized them to distinguish four time-dependent dark energy (TDDE) [50–57] scenarios and the  $\Lambda$ CDM scenario from each other. Except the statefinder hierarchy,  $Om$  diagnostic [58] and fractional growth parameter  $\epsilon$  of matter perturbations [48, 59, 60] could also be used to discriminating different dark energy models.  $Om$  can be constructed from the Hubble parameter  $H$  and it remains invariable at different stages of the universe for the  $\Lambda$ CDM model. Therefore, this diagnostic gives a simple null test to discriminate the  $\Lambda$ CDM scenario from the evolving dark energy models, since  $Om$  for various cosmological models are functions of redshift or scale factor. The fractional growth parameter  $\epsilon$  can be regarded as a supplement for statefinder hierarchy and usually used in conjunction with statefinder hierarchy to define a composite null diagnostic [48].

Each of three diagnostics gives a trajectory in phase diagram for one dark energy model. As will be shown in subsequent section, these diagnostics can be expressed in terms of some fundamental quantities, the EOS of dark energy  $w$ , the fractional density of dark energy  $\Omega_{de}$  (or baryons  $\Omega_m$ ), and the scalar factor  $a(t)$ . In [49], authors constrain TDDE models by

\* lxxu@dlut.edu.cn

using Type Ia supernovae (SNIa), baryonic acoustic oscillations (BAO), observational Hubble parameter (OHD) data sets as well as single data point from the newest event GW150914, they obtained best fitting values of model parameters  $\{\Omega_{m0}, w_0, w_i\}$  in TDDE models. However, they dropped error bars unwarily. It is possible for those diagnostics that may be very sensitive with these model parameters. The trajectories should have error bars at  $1\sigma$  or more higher confidence levels. It is meaningless when there is only best fitting values without error bars. Most of authors focused on these diagnostics only in the theoretical perspective without observational data, or someone used observational data to constrain their models, but no one considered the errors of the diagnostics that carried from the original variables. Hence, we will constrain three TDDE models by using more observational data sets, and analyze their diagnostics in terms of the new values of model parameters with error bars via the error propagation equation. This is the first time to introduce the error propagation equation into the model diagnostic mechanism. In this way, the trajectories in phase diagram will be replaced by regions. It is worth to expect that more information about the difference of models would be revealed through this new idea.

This paper is organized as follows. In the Section II, three joint diagnostics, statefinder hierarchy, fractional growth parameter  $\epsilon$  and  $Om$ , are recast into new expressions which modified by the error propagation equation. At the same time, some essential review about three TDDE models is stated. In Section III, by using the Markov Chain Monte Carlo (MCMC) method with currently available cosmic observational data sets *Planck* 2015, SNIa, BAO, and OHD, we constrain the models parameters and obtain the covariance matrixes. Then in Section IV, we discriminate and analyse three TDDE models by using the amendatory diagnostics. A summary is presented in the last section.

## II. THREE DIAGNOSTICS WITH ERROR BARS FOR THREE TDDE MODELS

Usually, cosmologists regard dark energy as a kind of ideal fluid, thus its physical properties can be characterized by EOS  $w$ , and fractional density  $\Omega_{de}$  on background level. Generally speaking, they are all functions of cosmic time  $t$  or scale factor  $a$ . By solving the Friedmann equation and the conservation equation, one can get the relation between the geometrical variable  $H$  and the dynamical quantities

$$E^2(a) \equiv \frac{H^2(a)}{H_0^2} = \Omega_{m0}a^{-3} + (1 - \Omega_{m0}) \exp\left\{-3 \int_1^a \frac{1 + w(\tilde{a})}{\tilde{a}} d\tilde{a}\right\}, \quad (2)$$

where  $E(a)$  is the dimensionless Hubble parameter. Because of both energy densities of the baryons and the cold dark matter (CDM) evolve proportional to  $a^{-3}$ , we express their density at present period together in terms of  $\Omega_{m0}$ . Then  $\Omega_{de0} \equiv 1 - \Omega_{m0}$  can be read immediately. The radiations have been neglected since we focus on the last-time acceleration.

Another important geometrical variable, the deceleration parameter  $q$ , can be expressed by those two physical quantities as

$$q \equiv -a\ddot{a}/\dot{a}^2 = \frac{1}{2}(1 + 3w(a)\Omega_{de}(a)), \quad (3)$$

where

$$\Omega_{de}(a) = \frac{E^2(a) - \Omega_{m0}a^{-3}}{E^2(a)} \quad (4)$$

is the relation of the fractional density of dark energy evolving over the scale factor  $a$ . By the definition of the statefinder,  $r$ ,  $s$  can be obtained from the derivative of deceleration parameter,

$$r = q(1 + 2q) - a \frac{dq}{da}, \quad (5)$$

$$s = \frac{r - 1}{3(q - 1/2)}. \quad (6)$$

However, to discriminate dark energy models better, Arabsalmani et al. proposed statefinder hierarchy as a new generation of diagnostic, which contains higher derivatives of the scale factor. We define a dimensionless quantity as

$$A_n \equiv \frac{a^{(n)}}{aH^n}, \quad (7)$$

where  $a^{(n)} = d^n a / dt^n$ . We follow the authors of [49] and define statefinder hierarchy  $S_n$  as

$$S_2 = A_2 + \frac{3}{2}\Omega_m(a), \quad (8)$$

$$S_3 = A_3, \quad (9)$$

$$S_4 = A_4 + \frac{3^2}{2}\Omega_m(a), \quad (10)$$

$$S_5 = A_5 - 3\Omega_m(a) - \frac{3^2}{2}\Omega_m^2(a), \quad \dots \quad (11)$$

This statefinder hierarchy  $S_n$  can be improved sequentially to another version  $S_n^{(1)}$  to reply more complicated models,

$$S_3^{(1)} = S_3, \quad (12)$$

$$S_4^{(1)} = A_4 + 3(1 + q), \quad (13)$$

$$S_5^{(1)} = A_5 - 2(4 + 3q)(1 + q), \quad \dots \quad (14)$$

It is easy to verify that both hierarchies have the same property for the fiducial cosmology, that is

$$S_n^{(1)}|_{\Lambda\text{CDM}} = S_n|_{\Lambda\text{CDM}} = 1. \quad (15)$$

Therefore, for  $\Lambda\text{CDM}$  cosmology, the pair of statefinder have an apparent expression  $\{S_n, S_n^{(1)}\}|_{\Lambda\text{CDM}} = (1, 1)$  on the phase diagram. The second member of statefinder hierarchy can be constructed from  $S_n^{(1)}$  in the following way [48],

$$S_n^{(2)} = \frac{S_n^{(1)} - 1}{3(q - \frac{1}{2})}. \quad (16)$$

Recently, in a series of articles, researchers studied various dark energy models by using those statefinder hierarchies. However, we inspect those statefinder hierarchies from another perspective, i.e. the error bars. We take two pairs of

them,  $\{S_3^{(1)}, S_4^{(1)}\}$  and  $\{S_5^{(1)}, S_5^{(2)}\}$ , as examples to illustrate the influence of the error bars on the results of distinguishing dark energy models. The concrete formulas of those statefinders in terms of the cosmological parameters can be written as

$$S_3^{(1)} = A_3 = r, \quad (17)$$

$$A_4 = r - 3(q+1)r + a \frac{dr}{da}, \quad (18)$$

$$S_4^{(1)} = r - 3(q+1)r + a \frac{dr}{da} + 3(1+q), \quad (19)$$

$$A_5 = A_4 - 4(q+1)A_4 + a \frac{dA_4}{da}, \quad (20)$$

$$S_5^{(1)} = A_5 - 2(4+3q)(1+q), \quad (21)$$

$$S_5^{(2)} = \frac{S_5^{(1)} - 1}{3(q-\frac{1}{2})}. \quad (22)$$

Those formulas are all functions of  $\Omega_{m0}$ ,  $w(a)$  and  $a$ . In this paper, we parameterize EOS  $w(a)$  in the following three time-dependent ways,

$$w(a) = w_0 + w_1 \ln a, \quad (23)$$

$$w(a) = w_0 + w_2(1-a), \quad (24)$$

$$w(a) = w_0 + w_3 \frac{1-a}{a^2+(1-a)^2}, \quad (25)$$

where  $w_0$  denotes the present ( $a=1$ ) value of  $w(a)$ . (23) (24) (25) correspond to models 1, 2, 3 respectively.  $w_0$ ,  $w_i$  and  $\Omega_{m0}$  are all free parameters for each model, thus they should be estimated by observational data sets. By using the Markov Chain Monte Carlo (MCMC) method in Section III, these parameters are coming with error bars. The errors would propagate from these parameters to the statefinders via the error propagation equation.

Generally speaking in statistics, people usually use a  $n$  dimension vector  $\mathbf{X} = (X_1, X_2, \dots, X_n)^T$  to express  $n$  random variables which can be obtained directly. And  $\mu = (\mu_1, \mu_2, \dots, \mu_n)^T \equiv E(\mathbf{X})$  is the expected value vector of  $\mathbf{X}$ . For certain function  $f$  of the  $n$  random variables, the square error  $\sigma_f^2$  of  $f$  can be given by the following formula

$$\begin{aligned} \sigma_f^2 &\approx \sum_{i=1}^n \sum_{j=1}^n \left( \frac{\partial f}{\partial X_i} \frac{\partial f}{\partial X_j} \right)_{\mathbf{X}=\mu} Cov(X_i, X_j) \\ &= \sum_{i=1}^n \left( \frac{\partial f}{\partial X_i} \right)_{\mathbf{X}=\mu}^2 Cov(X_i, X_i) \\ &\quad + 2 \sum_{i<j}^n \left( \frac{\partial f}{\partial X_i} \frac{\partial f}{\partial X_j} \right)_{\mathbf{X}=\mu} Cov(X_i, X_j), \end{aligned} \quad (26)$$

where  $Cov(X_i, X_j) \equiv Cov(X_j, X_i)$  is the covariance matrix of  $n$  random variables. Then  $f$  with error bar should be rewritten as  $f \pm \sigma_f$ . In this work, we consider a three dimension vector of random variances  $(\Omega_{m0}, w_0, w_i)$ , and the corresponding covariance matrix can be generated during MCMC. When adding error bars in the phase diagram, it should be regions rather than trajectories. The positional relationships of these regions would be multifarious, and more information about dark energy models can be unscramble than before.

Except statefinder hierarchies, we consider two more diagnostics with error bars to discriminate and analyse dark energy

models as complements. One is fractional growth parameter  $\epsilon(a)$ ,

$$\epsilon(a) = \frac{f(a)}{f_{\Lambda\text{CDM}}(a)}, \quad (27)$$

where

$$f(a) = \Omega_m(a)^{\gamma(a)}, \quad (28)$$

is the growth rate of perturbations. In our TDDE models, the variation of  $w(a)$  is slow enough so that the condition  $|dw/d\Omega_m| \ll (1 - \Omega_m)^{-1}$  is satisfied, meanwhile since the present value of  $1 - \Omega_m$  is not really small, the following approximate estimate for  $\gamma$  can be used [13],

$$\gamma(a) \approx \frac{3}{5 - \frac{w}{1-w}} + \frac{3}{125} \frac{(1-w)(1-1.5w)}{(1-1.2w)^3} [1 - \Omega_m(a)]. \quad (29)$$

Note that the  $\Lambda\text{CDM}$  model corresponds to  $\gamma \approx 6/11 \approx 0.545$ . It is useful to remark that while  $\gamma$  does not depend strongly on  $w(a)$ , the rate  $f = \Omega_m^\gamma$  is significantly affected by  $w(a)$ . Another is  $Om$  diagnostic [58] which is constructed by the dimensionless Hubble parameter in the following way

$$Om(a) \equiv \frac{E^2(a) - 1}{a^{-3} - 1}, \quad (30)$$

where  $E(a)$  has been given in (2). It is obviously that for the fiducial cosmology, one has

$$Om(a) |_{\Lambda\text{CDM}} = \Omega_{m0}. \quad (31)$$

Analogously, the error bars of  $\epsilon(a)$  and  $Om(a)$  can be obtained via the error propagation equation (26). It would be efficient to recombine these three diagnostics into some combinations.

### III. THE CONSTRAINTS ON MODELS

Diagnostics with error bars for three TDDE models have been analyzed in previous section. Anyway any conjecture should be supported by the cosmic observations. Subsequently a global fitting for those models by using the cosmic observational data sets from *Planck* 2015 [12] low- $l$ , TT, EE, TE, lensing, joint SNIa [61–63], BAO [64–67], OHD [68, 69] would be performed. Wang et al. [49] constrained four TDDE models using the last three data sets. Here we add *Planck* 2015 data set and expect to get a more compact constraint on the parameter spaces for our three TDDE models. More important, Wang et al. dropped the error bars, so it is necessary to obtain the error bars as well as the covariance matrixes to continue our work. According to the publicly available CosmoMC package [70], the total likelihood  $\chi^2$  can be constructed as

$$\chi^2 = \chi_{Planck}^2 + \chi_{SNIa}^2 + \chi_{BAO}^2 + \chi_{OHD}^2, \quad (32)$$

where the four terms in right side of this equation, denote the contributions from *Planck* 2015, SNIa, BAO, OHD data sets

respectively. The parameter spaces for the models considered in this paper is given by

$$P_i = \{\Omega_{m0}, w_0, w_i\}, \quad (33)$$

where  $i = 1, 2, 3$  corresponding to three TDDE models.

After running eight chains in parallel on computer, the mean values with errors and best-fit values, respectively, are presented in TABLE I, II, III, for three models respectively. One dimensional (1D) marginalized distributions of parameters and 2D contours with 68% C.L., 95% C.L., and 99.7% C.L. are presented in FIG. 1, 2, 3.

Parameters	Mean with errors	Best fit
$\Omega_{m0}$	$0.313^{+0.00971+0.0195+0.0257}_{-0.00971-0.0190-0.0245}$	0.315
$w_0$	$-0.902^{+0.0635+0.151+0.210}_{-0.0859-0.138-0.161}$	-0.925
$w_1$	$0.275^{+0.0694+0.364+0.537}_{-0.275-0.275-0.275}$	0.112

TABLE I. The mean values with  $1\sigma$ ,  $2\sigma$ ,  $3\sigma$  error bars and best-fit values for the parameter space of model 1.

Parameters	Mean with errors	Best fit
$\Omega_{m0}$	$0.313^{+0.00958+0.0191+0.0249}_{-0.00957-0.0186-0.0243}$	0.309
$w_0$	$-0.899^{+0.0677+0.153+0.200}_{-0.0883-0.141-0.167}$	-0.948
$w_2$	$-0.366^{+0.366+0.366+0.366}_{-0.102-0.455-0.633}$	-0.127

TABLE II. The mean values with  $1\sigma$ ,  $2\sigma$ ,  $3\sigma$  error bars and best-fit values for the parameter space of model 2.

Parameters	Mean with errors	Best fit
$\Omega_{m0}$	$0.313^{+0.00961+0.0195+0.0257}_{-0.00959-0.0185-0.0238}$	0.311
$w_0$	$-0.913^{+0.0629+0.137+0.184}_{-0.0759-0.130-0.155}$	-0.961
$w_3$	$-0.177^{+0.177+0.177+0.177}_{-0.0487-0.223-0.322}$	-0.0933

TABLE III. The mean values with  $1\sigma$ ,  $2\sigma$ ,  $3\sigma$  error bars and best-fit values for the parameter space of model 3.

The CosmoMC also generates covariance matrixes for the vector of random variables. The covariance coefficients of  $(\Omega_{m0}, w_0, w_i)$  are displayed in matrix form (34), (35), (36) for three models respectively, which are all on  $1\sigma$  confidence level.

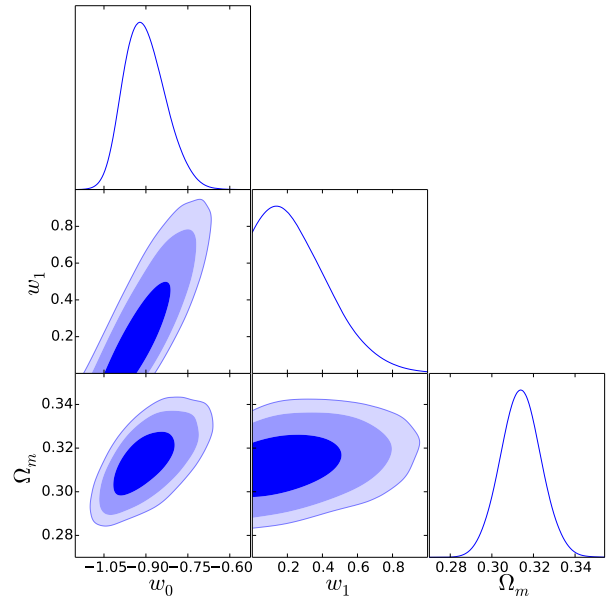


FIG. 1. 1D marginalized distributions on individual parameters and 2D contours with 68% C.L., 95% C.L., and 99.7% C.L. between each other for the parameter space of model 1.

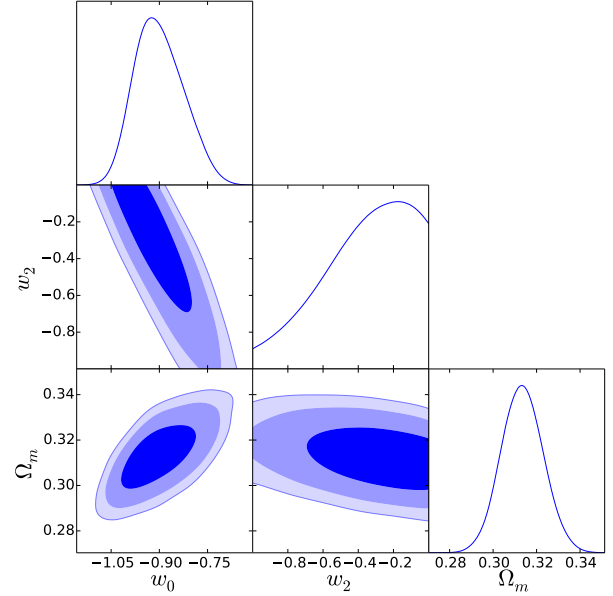


FIG. 2. 1D marginalized distributions on individual parameters and 2D contours with 68% C.L., 95% C.L., and 99.7% C.L. between each other for the parameter space of model 2.

$$Cov_1 = \begin{pmatrix} 8.659 \times 10^{-6} & -1.449 \times 10^{-5} & 1.99 \times 10^{-4} \\ -1.449 \times 10^{-5} & 5.509 \times 10^{-3} & 1.111 \times 10^{-2} \\ 1.99 \times 10^{-4} & 1.111 \times 10^{-2} & 3.631 \times 10^{-2} \end{pmatrix}, \quad (34)$$

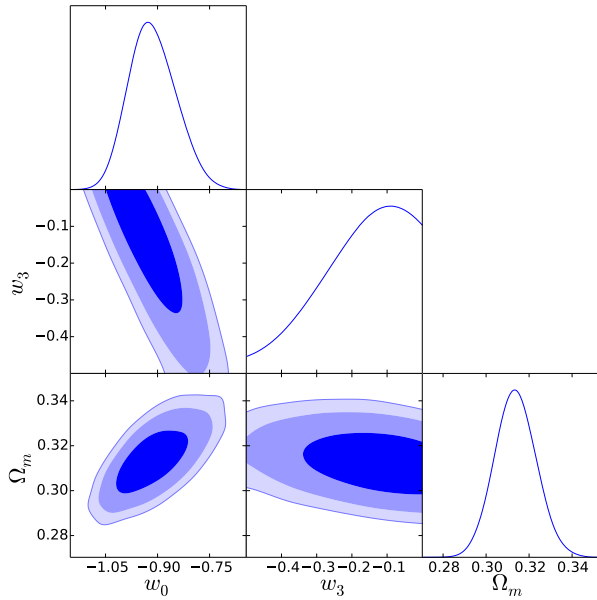


FIG. 3. 1D marginalized distributions on individual parameters and 2D contours with 68% C.L., 95% C.L., and 99.7% C.L. between each other for the parameter space of model 3.

$$Cov_2 = \begin{pmatrix} 8.203 \times 10^{-6} & -1.932 \times 10^{-5} & -2.228 \times 10^{-4} \\ -1.932 \times 10^{-5} & 5.76 \times 10^{-3} & -1.47 \times 10^{-2} \\ -2.228 \times 10^{-4} & -1.47 \times 10^{-2} & 5.804 \times 10^{-2} \end{pmatrix}, \quad (35)$$

$$Cov_3 = \begin{pmatrix} 8.372 \times 10^{-6} & -3.241 \times 10^{-5} & -1.066 \times 10^{-4} \\ -3.241 \times 10^{-5} & 4.623 \times 10^{-3} & -5.942 \times 10^{-3} \\ -1.066 \times 10^{-4} & -5.942 \times 10^{-3} & 1.392 \times 10^{-2} \end{pmatrix}. \quad (36)$$

#### IV. ANALYSIS ON MODELS BY USING THE ADVANCED DIAGNOSTICS

In this section, we substitute the best-fit values of the random variables ( $\Omega_{m0}$ ,  $w_0$ ,  $w_i$ ) in TABLE I, II, III, and the covariance matrices (34), (35), (36) obtained in Section III into the diagnostics  $S_3^{(1)}$  (17),  $S_4^{(1)}$  (19),  $S_5^{(1)}$  (21),  $S_5^{(2)}$  (22),  $\epsilon$  (27),  $Om$  (30) with the error propagation equation (26) stated in Section II, then we get the modified phase diagrams of these diagnostics. The original phase diagrams without error bars are displayed as a comparison to see improvements on discriminating different dark energy. It is worth noting that we ignore the correlation between the diagnostics. Actually, each point in the phase diagram represents a temporal state of a dark energy model. The point should be replaced by a cross when one adds error bars, and further become a contour when one considers correlation between the diagnostics. In the last case, it is not too hard to imagine what phase diagram appeared when

scale factor  $a$  or redshift  $z$  varies, but it is hard to visualization. So we consider error bars without correlation in our work, and convince that it is enough to achieve our purpose.

The phase diagram of  $\{S_3^{(1)}, S_4^{(1)}\}$  without error bars for three models is showed in FIG. 4. It is obviously that all three models together with the  $\Lambda$ CDM can be well distinguished from each other at the present period. FIG. 5 is the modified version with  $1\sigma$  error bars. In this figure, the red region (model 2) almost completely covers two remaining colors at the epoch of  $a$  from  $e^{-2}$  to  $e^{0.2}$ , including the present period. So we can say that the statefinder pair  $\{S_3^{(1)}, S_4^{(1)}\}$  can not discriminate model 1 and model 3 from model 2 in  $1\sigma$  confidence level. Even model 1 and model 2 share the similar evolutionary tendency in FIG. 4, their behaviours with  $1\sigma$  error bars are quite different. Brushing aside the red region, the green one (model 1) and the blue one (model 3) can discriminate from each other at some points. By carefully inspecting we note that the blue point is located in the region centered by the green point, which means it is reluctantly to discriminate the model 3 from model 1 in present period.

Then we investigate the phase diagram of  $\{S_3^{(1)}, \epsilon\}$  without and with error bars in FIG. 6 and FIG. 7 respectively. Similar with FIG. 4, these three models and the  $\Lambda$ CDM can be distinguished easily in FIG. 6. Model 1 and model 2 have a similar evolutionary tendency. This behavior is also reflected in FIG. 7, that is, the region of green and red almost superpose. But for the blue one, there is an obviously deviation from the other two at the preliminary period. This feature can help us to distinguish the model 3 from the other two models.

FIG. 8 and FIG. 9 are the phase diagram of  $\{S_4^{(1)}, \epsilon\}$ . Similar analysis can be obtained in this case. From all three pairs of diagnostics we can summarize that model 2 has the broadest region than the other two and model 3 can be distinguished from the remaining two to some extent.

Then subsequently we investigate the other three pairs of diagnostics,  $\{S_5^{(1)}, S_5^{(2)}\}$ ,  $\{S_5^{(1)}, \epsilon\}$ , and  $\{S_5^{(2)}, \epsilon\}$  in the same way. FIG. 10 is the phase diagram of  $\{S_5^{(1)}, S_5^{(2)}\}$  without error bars. It is easy to see that the blue point quite closes to the black point, which means that this pair of statefinders can not distinguish model 3 from the  $\Lambda$ CDM model, but there is no problem for the other two models. It is worth noting that model 3 will go through the fixed point (1, 0) which corresponds to the  $\Lambda$ CDM scenario more than one time which means the stability of this system is good. In FIG. 11 we can see that the red region and the blue region tend to the opposite direction and the distance between the red and the blue points are so far away from each other's  $1\sigma$  region in present period that these two models can be distinguished very well. The green region mediates between the other two so that the status is equivocal. FIG. 12, 13, 14, 15 verify our analysis above.

Synthesizes the above analysis, the combination of  $S_5^{(1)}, S_5^{(2)}, \epsilon$  is better than the combination of  $S_3^{(1)}, S_4^{(1)}, \epsilon$ . From all six phase diagrams without error bars, we can see model 1, model 2 share the similar evolutionary tendency, and the trajectory of model 3 is quite different to them. Model 3 more closes to the  $\Lambda$ CDM cosmology. All six phase diagrams with  $1\sigma$  error bars verify this and the region of model 3 is more compact

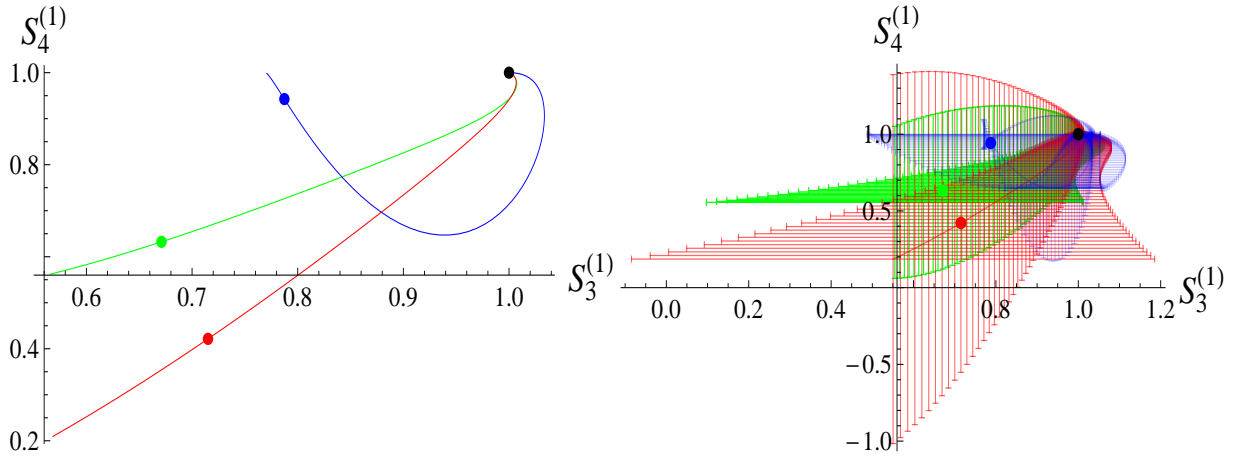


FIG. 4. (left) The phase diagram of  $\{S_3^{(1)}, S_4^{(1)}\}$  without error bars. The green, red, blue line correspond to model 1, model 2, model 3 and the points label the present situations respectively. Specifically, the black point denotes the  $\Lambda$ CDM model. The values of  $a$  range from  $e^{-2}$  to  $e^{0.2}$ .

FIG. 5. (right) The phase diagram of  $\{S_3^{(1)}, S_4^{(1)}\}$  with error bars. The others are same with the left panel.

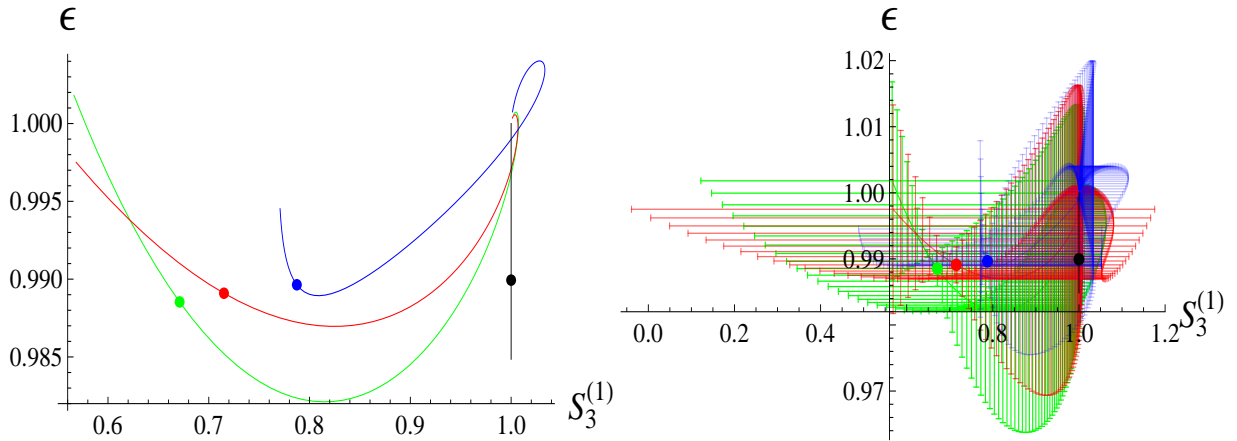


FIG. 6. (left) The phase diagram of  $\{S_3^{(1)}, \epsilon\}$  without error bars. The green, red, blue line correspond to model 1, model 2, model 3 and the points label the present situations respectively. Specifically, the black point denotes the  $\Lambda$ CDM model. The values of  $a$  range from  $e^{-2}$  to  $e^{0.2}$ .

FIG. 7. (right) The phase diagram of  $\{S_3^{(1)}, \epsilon\}$  with  $1\sigma$  error bars. The others are same with the left panel.

than the other two. This system is so robust to resist the errors generated from the original parameters. The distribution of model 2 is the broadest which means the errors are easy to propagate from the original parameters, so we can say that this system is unstable. By using these two types (with and without error bars) of diagnostic, we distinguish three TDDE dark energy models successfully and even more screen out the better model.

The last figure is the relation between redshift and  $Om$  with  $1\sigma$  error bars. The error bars of all three models are short at large  $z$ , and trend to broad while  $z$  becomes smaller. This means these systems in early time are more stable than in later time. For individual model, the blue region is the most compact one and covered by the other two which verify model 3

is the most robust again. The tendency of the blue center line is almost as placid as the black one, and this also confirm that model 3 is so much alike with the  $\Lambda$ CDM.

## V. CONCLUSION

The most important mission in cosmology now is to interpret the last-time cosmic acceleration. For this purpose, cosmologists have proposed various of mechanisms, including many dark energy models. Most of these dark energy models possess analogous geometric behaviours on background, thus how to distinguish those models from geometric and dynamical aspects, and further more, to judge a model is better

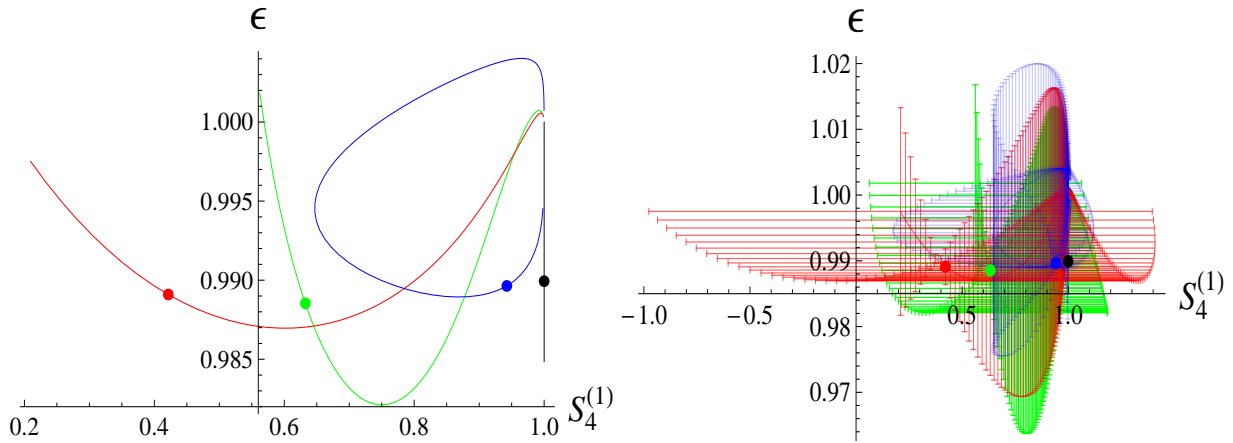


FIG. 8. (left) The phase diagram of  $\{S_4^{(1)}, \epsilon\}$  without error bars. The green, red, blue line correspond to model 1, model 2, model 3 and the points label the present situations respectively. Specifically, the black point denotes the  $\Lambda$ CDM model. The values of  $a$  range from  $e^{-2}$  to  $e^{0.2}$ .

FIG. 9. (right) The phase diagram of  $\{S_4^{(1)}, \epsilon\}$  with  $1\sigma$  error bars. The others are same with the left panel.

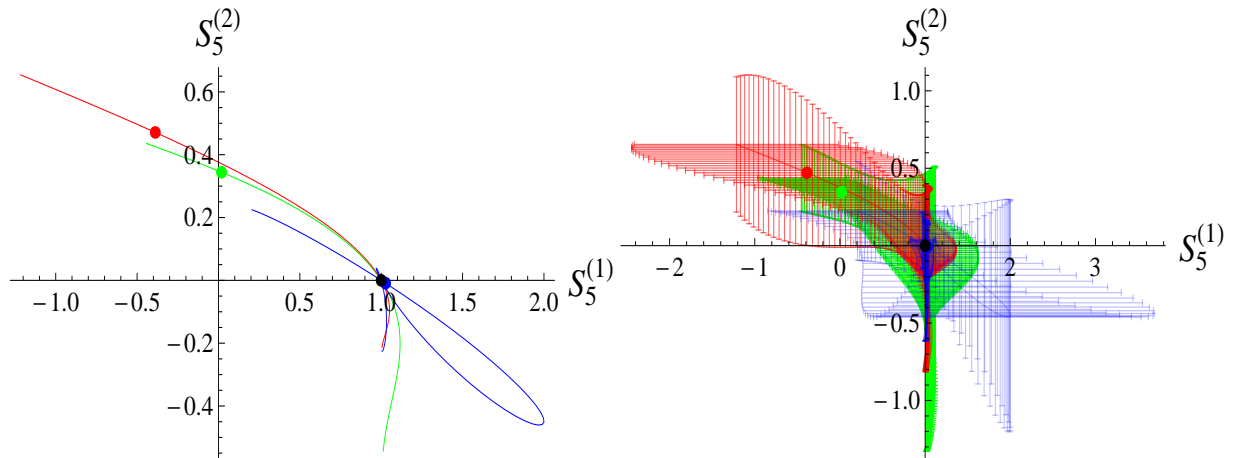


FIG. 10. (left) The phase diagram of  $\{S_5^{(1)}, S_5^{(2)}\}$  without error bars. The green, red, blue line correspond to model 1, model 2, model 3 and the points label the present situations respectively. Specifically, the black point denotes the  $\Lambda$ CDM model. The values of  $a$  range from  $e^{-2}$  to  $e^{0.3}$ .

FIG. 11. (right) The phase diagram of  $\{S_5^{(1)}, S_5^{(2)}\}$  with  $1\sigma$  error bars. The others are same with the left panel.

then another one or not has become an important issue. Since Sahni et al. proposed the statefinder, researchers studied many dark energy models by using it. And in order to distinguish and judge better, more diagnostics, such as the hierarchy of statefinder in higher derivative, fractional growth parameter  $\epsilon$  and  $Om$  diagnostic, have been proposed. Over the years, researchers obtained abundant achievements in this field.

However, most of researchers considered these diagnostics only in theoretical perspective without observational datas, or someone used observational data but ignored the error bars of cosmological parameters. To change this awkward situation, we did the following three works: to modify the diagnostics with error bars via the error propagation equation (Section II), to constrain three TDDE models by using cosmic observa-

tional data sets from *Planck* 2015 low- $l$ , TT, EE, TE, lensing, joint SNIa, BAO, OHD (Section III), and to distinguish and judge three TDDE models by using the modified diagnostics with fresh best fit values and covariance matrices (Section IV). Some conclusions could be drawn after a detailed analysis.

Firstly the trajectories of model 3 are quite different from model 1 and model 2 in the phase diagrams without error bars (FIG. 4, FIG. 6, FIG. 8, FIG. 10, FIG. 12, FIG. 14). Model 3 is more approximate to  $\Lambda$ CDM cosmology in present period (FIG. 10, FIG. 12, FIG. 14), and its trajectory can go through the fixed point (1, 0) which corresponds to the  $\Lambda$ CDM scenario more than one time (FIG. 10) which means the stability of this system is better than the other two. From the phase diagrams with error bars (FIG. 5, FIG. 7, FIG. 9, FIG.

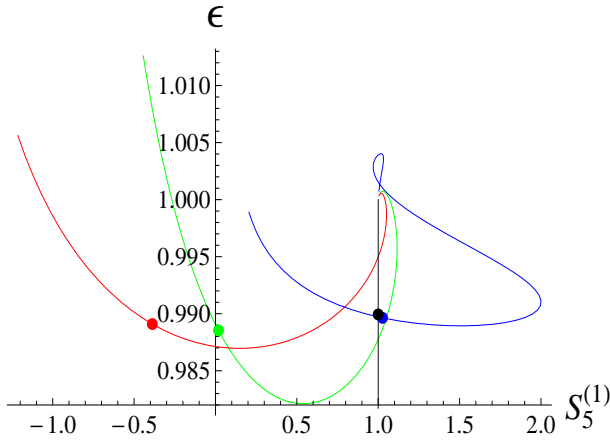


FIG. 12. (left) The phase diagram of  $\{S_5^{(1)}, \epsilon\}$  without error bars. The green, red, blue line correspond to model 1, model 2, model 3 and the points label the present situations respectively. Specifically, the black point denotes the  $\Lambda$ CDM model. The values of  $a$  range from  $e^{-2}$  to  $e^{0.3}$ .

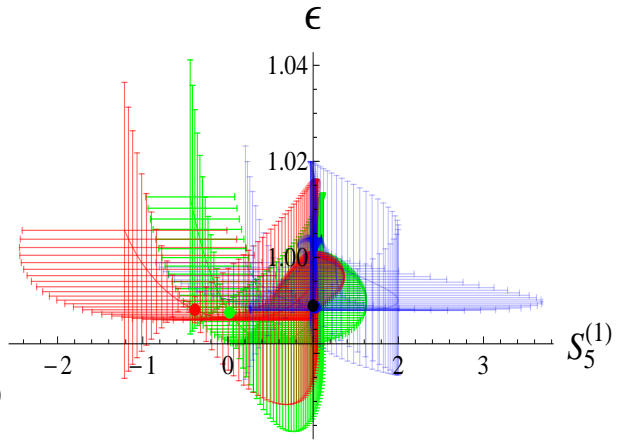


FIG. 13. (right) The phase diagram of  $\{S_5^{(1)}, \epsilon\}$  with  $1\sigma$  error bars. The others are same with the left panel.

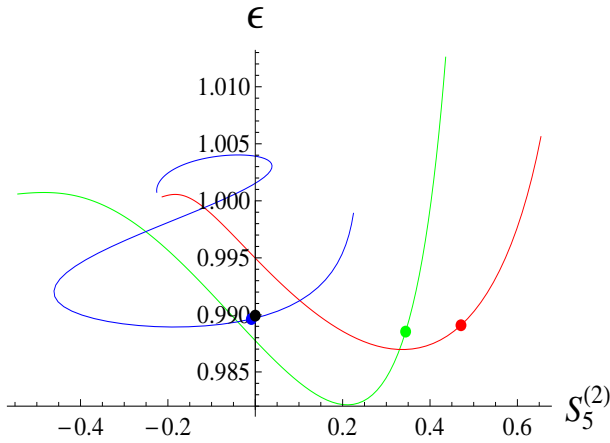


FIG. 14. (left) The phase diagram of  $\{S_5^{(2)}, \epsilon\}$  without error bars. The green, red, blue line correspond to model 1, model 2, model 3 and the points label the present situations respectively. Specifically, the black point denotes the  $\Lambda$ CDM model. The values of  $a$  range from  $e^{-2}$  to  $e^{0.3}$ .

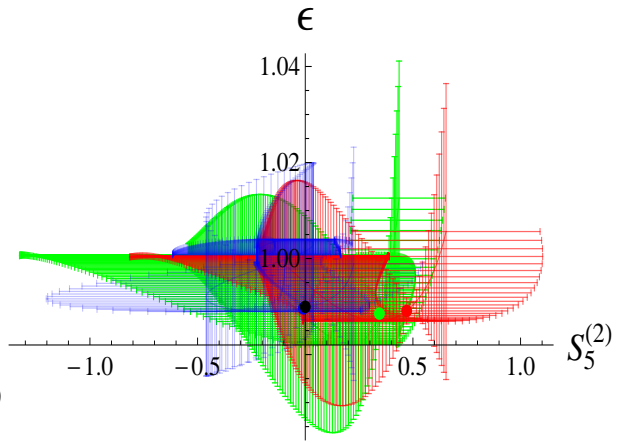


FIG. 15. (right) The phase diagram of  $\{S_5^{(2)}, \epsilon\}$  with  $1\sigma$  error bars. The others are same with the left panel.

15), we found the  $1\sigma$  region of model 3 is more compact than the other two regions which means this system is so robust to resist the errors generating from the original parameters and model 2 is the most unstable one as a comparison. FIG. 7, FIG. 11, FIG. 13 show that model 3 can be distinguished from the other two to some extent. Then by contrasting the phase diagrams of two combinations of diagnostic,  $S_3^{(1)}, S_4^{(1)}, \epsilon$  and  $S_5^{(1)}, S_5^{(2)}, \epsilon$ , we found that the last combination is better to distinguish three TDDE models. That is the reason why people proposed higher derivative hierarchy of statefinders as the new diagnostics. At last, the analysis on  $Om$  can be regarded as a supplement and verification for above three.

However, there are defects in our work yet and several arrangement should be done to perfect it in the future. We ig-

nored the correlation between the diagnostics. As a dynamical phase diagram, it will be better if we give the contour at certain moment (for instance in present period) for every model. These three TDDE models are a little simple and weak, but here we focus on the modified diagnostics with error bars so it is enough in this sense. We will try to use the new diagnostics to distinguish and investigate more dark energy models subsequently. The quality and quantity of the observational data sets which we used should be improved. The contours FIG. 1, 2, 3 and the covariance coefficients in (34), (35), (36) show straightway that the order of compactness for three constraints from high to low is model 3 > model 1 > model 2, which is consistent with the results obtained via the error propagation equation. The effects of the error propagation equation

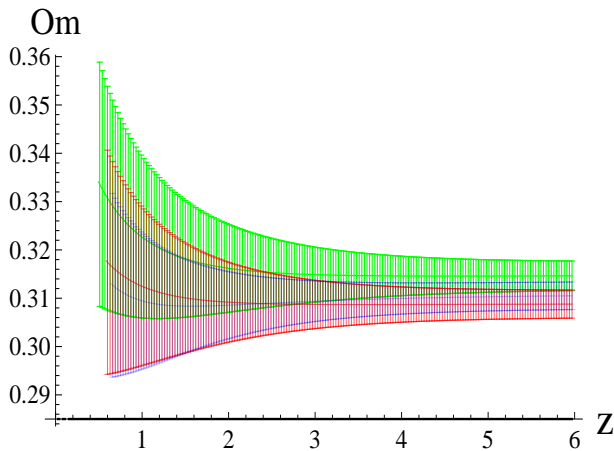


FIG. 16. The relation between the redshift and  $Om$  with  $1\sigma$  error bars. The green, red, blue and black line correspond to model 1, model 2, model 3 and the  $\Lambda$ CDM model respectively.

are weakened because of this degeneracy. For eliminating this negative influence, an absolute comparison among models should be carried out via bayesian methods. This will be our subsequent work.

## ACKNOWLEDGMENTS

We thank an anonymous referee for helpful improvement of this paper. L. Xu's work is supported in part by NSFC under the Grants No. 11275035.

- 
- [1] A. G. Riess *et al.*, *Astrophys. J.* **116**, 1009 (1998).  
[2] S. Perlmutter *et al.*, *Astrophys. J.* **517**, 565 (1999).  
[3] D. N. Spergel *et al.*, *Astrophys. J. Suppl. Ser.* **148**, 175 (2003).  
[4] M. Tegmark *et al.*, *Astrophys. J.* **606**, 702 (2004).  
[5] S. Weinberg, *Rev. Mod. Phys.* **61**, 1 (1989).  
[6] V. Sahni, and L. Wang, *Phys. Rev. D* **62**, 103517 (2000).  
[7] S. M. Carroll, *Living Rev. Rel.* **4**, 41 (2001).  
[8] P. J. E. Peebles, and B. Ratra, *Rev. Mod. Phys.* **75**, 559 (2003).  
[9] T. Padmanabhan, *Physics Reports* **380**, 235 (2003).  
[10] E. J. Copeland, M. Sami, and S. Tsujikawa, *Int. J. Mod. Phys. D* **15**, 1753 (2006).  
[11] M. Li, X. D. Li, and S. Wang *et al.*, World Scientific Publishing Company (2014).  
[12] Planck Collaboration. *Planck* 2015 results. XIII. arXiv:1502.01589.  
[13] L. Amendola, and S. Tsujikawa, Cambridge University Press (2010).  
[14] R. R. Caldwell, *Phys. Lett. B* **545**, 23 (2002).  
[15] R. R. Caldwell, M. Kamionkovski, and N. N. Weinberg, *Phys. Rev. Lett.* **91**, 071301 (2003).  
[16] Y. F. Cai, *Physics Reports* **493**, 1 (2010).  
[17] X. Dou, and X. H. Meng, *Adv. Astron.* **1155**, 829340 (2011).  
[18] M. Malekjani, *Astrophys. Space. Sci.* **334**, 193 (2011).  
[19] J. B. Lu *et al.*, *JHEP* **2**, 71 (2015).  
[20] R. J. Yang, *Phys. Rev. D* **89**, 063014 (2014).  
[21] P. Wang, and X. H. Meng, *Class. Quant. Grav.* **22**, 283 (2005).  
[22] X. Zhang, and H. Liu, *Phys. Lett. B* **659**, 26 (2008).  
[23] A. Pasqua *et al.*, *Astrophys. Space. Sci.* **340**, 199 (2012).  
[24] J. Ren, and X. H. Meng, *Int. J. Mod. Phys. D* **17**, 2325 (2008).  
[25] S. M. Carroll *et al.*, *Phys. Rev. D* **70**, 043528 (2004).  
[26] P. Ruiz-Lapuente, *Class. Quant. Grav.* **24**, R91 (2007).  
[27] L. Amendola *et al.*, *JCAP* **0612**, 020 (2006).  
[28] T. Jacobson, *Phys. Rev. D* **81**, 101502 (2010).  
[29] V. Sahni, and Y. Shtanov, *JCAP* **0311**, 014 (2003).  
[30] V. Sahni, T. D. Saini, A. A. Starobinsky, and U. Alam, *JETP Lett.* **77**, 201 (2003).  
[31] V. Sahni, T. D. Saini and A. A. Starobinsky, *MNRAS* **344**, 1057 (2003).  
[32] S. Chongchitnan, and G. Efstathiou, *Phys. Rev. D* **76**, 043508 (2007).  
[33] E. V. Linder, *Gen. Rel. Grav.* **40**, 329 (2008).  
[34] V. Gorini, A. Kamenshchik, and U. Moschella, *Phys. Rev. D* **67**, 063509 (2003).  
[35] P. Wu, and H. Yu, *Int. J. Mod. Phys. D* **14**, 1873 (2005).  
[36] G. Yang, D. Wang, and X. H. Meng, arXiv:1602.02552.  
[37] X. T. Gao, and R. J. Yang, *Phys. Lett. B* **687**, 99 (2010).  
[38] W. Chakraborty, U. Debnath, and S. Chakraborty, *Grav. Cosmol.* **13**, 294 (2007).  
[39] S. Li, Y. Ma, and Y. Chen, *Int. J. Mod. Phys. D* **18**, 1785 (2009).  
[40] L. N. Granda, W. Cardona, and A. Oliveros, arXiv:0910.0778v1.  
[41] J. Zhang, X. Zhang, and H. Liu, *Phys. Lett. B* **659**, 26 (2008).  
[42] C. J. Feng, *Phys. Lett. B* **670**, 231 (2008).  
[43] H. Wei, and R. G. Cai, *Phys. Lett. B* **655**, 1 (2007).  
[44] G. Panotopoulos, *Nucl. Phys. B* **796**, 66 (2008).  
[45] R. Myrzakulov, and M. Shahalam, *JCAP* **10**, 047 (2013).  
[46] M. Sami, M. Shahalam, M. Skugoreva, and A. Toporensky, *Phys. Rev. D* **86**, 103532 (2012).  
[47] S. Ghaffari, A. Sheykhi, and M. H. Dehghani, *Phys. Rev. D* **91**, 023007 (2015).  
[48] M. Arabsalmani, and V. Sahni, *Phys. Rev. D* **83**, 043501 (2011).  
[49] D. Wang, and X. H. Meng, arXiv: 1603.00699.  
[50] J. Weller, A. Albrecht, *Phys. Rev. D* **65**, 103512 (2002).  
[51] I. Maor *et al.*, *Phys. Rev. D* **65**, 123003 (2002).  
[52] M. Goliath *et al.*, *Astron. Astrophys.* **380**, 6 (2001).  
[53] G. Efstathiou, *MNRAS* **310**, 842 (1999).  
[54] M. Chevallier, and D. Polarski, *Int. J. Mod. Phys. D* **10**, 213 (2013).  
[55] E. V. Linder, *Phys. Rev. Lett.* **90**, 091301 (2003).  
[56] T. Padmanabhan, and T. R. Choudhury, *MNRAS* **344**, 823 (2003).  
[57] E. M. Barboza Jr *et al.*, *Phys. Lett. B* **666**, 415 (2008).  
[58] V. Sahni, A. Shafieloo, and A. A. Starobinsky, *Phys. Rev. D* **78**, 103502 (2008).  
[59] V. Acquaviva, A. Hajian, D. N. Spergel and S. Das, *Phys. Rev. D* **78**, 043514 (2008).

- [60] V. Acquaviva, and E. Gawiser, arXiv:1008.3392.
- [61] J. Guy *et al.*, *Astron. Astrophys.* **523**, A7 (2010).
- [62] A. Conley *et al.*, *Astrophys. J. Suppl.* **192**, 1 (2011).
- [63] M. Sullivan *et al.*, *Astrophys. J.* **737**, 102 (2011).
- [64] F. Beutler *et al.*, *Mon. Not. Roy. Astron. Soc.* **416**, 3017 (2011).
- [65] N. Padmanabhan *et al.*, *Mon. Not. Roy. Astron. Soc.* **427**, 2132 (2012).
- [66] M. Manera *et al.*, *Mon. Not. Roy. Astron. Soc.* **428**, 1036 (2013).
- [67] C. Blake *et al.*, *MNRAS* **418**, 1707 (2011).
- [68] T. J. Zhang *et al.*, *Adv. Astron.* 184284 (2010).
- [69] X. H. Meng, and X. L. Du, *Commun. Theor. Phys.* **57**, 2 (2012).
- [70] A. Lewis, and S. Bridle, *Phys. Rev. D* **66**, 103511 (2002); <http://cosmologist.info/cosmomc/>.